Mean-field treatment of the many-body Fokker–Planck equation

2001 J. Phys. A: Math. Gen. 34 11225

(http://iopscience.iop.org/0305-4470/34/50/305)

INSTITUTE OF PHYSICS PUBLISHING JOURNAL OF PHYSICS A: MATHEMATICAL AND GENERAL

J. Phys. A: Math. Gen. **34** (2001) 11225–11240 PII: S0305-4470(01)25670-4

Mean-field treatment of the many-body Fokker–Planck equation

Nicolas Martzel and Claude Aslangul

Groupe de Physique des Solides, Laboratoire associé au CNRS UMR 7588, Universités Paris 7 & Paris 6, Tour 23, 2 Place Jussieu, 75251 Paris Cedex 05, France

E-mail: martzel@gps.jussieu.fr and aslangul@gps.jussieu.fr

Received 11 June 2001, in final form 27 September 2001
Published 7 December 2001
Online at stacks.iop.org/JPhysA/34/11225

Abstract

We review some properties of the stationary states of the Fokker–Planck equation for N interacting particles within a mean-field approximation, which yields a non-linear integrodifferential equation for the particle density. Analytical results show that for attractive long-range potentials the steady state is always a precipitate containing one or several clusters of small size. For arbitrary potential, linear stability analysis allows the statement of the conditions under which the uniform equilibrium state is unstable against small perturbations and, via the Einstein relation, definition of a critical temperature T_c separating the two phases, uniform and precipitate. The corresponding phase diagram turns out to be strongly dependent on the pair-potential. In addition, numerical calculations reveal that the transition is hysteretic. We finally discuss the dynamics of relaxation for the uniform state suddenly cooled below T_c.

PACS numbers: 05.10.Gg, 02.30.−f, 02.60.Nm, 64.60.−i

1. Introduction

The dynamics of Brownian particles is a subject of great interest in statistical physics, especially when the particles interact through potentials that can be short or long range, from the simple hard-core to Coulombian interactions. The physics of surfaces, more precisely the motion of adatoms on substrates, provides an experimental realization of this problem. Interactions can lead to collective phenomena, and, generally speaking, to patterns in space. Pioneering studies have revealed experimental and computational evidence of a phase transition in the case of oxygen adsorbed on tungsten [1, 2]. This phase transition and the dynamics of such systems (e.g. the modification of the diffusion constant D of a tracer, time auto-correlation function of the on-site density, etc...) were analysed by Tringides *et al* [3] and reviewed by Gomer [4]. Numerical studies for a two-dimensional lattice gas have also been performed in the case of a contact interaction [5–7]. In a slightly different context, especially when

the considered system is an open one, many papers have been devoted to statistical models describing chemical reactions [8] (and references therein, especially the review by Zhdano and Kasemo [9]). All these works use a lattice gas framework (discrete space) based on a master equation; for details on two-dimensional lattice gas models (and their subsequent approximations), the review by Kehr and Binder [10] is highly recommended.

As is well known, the master equation with short-range jumps is just the discrete version of the ordinary Fokker–Planck equation (FPE). The latter results from the truncation of the Kramers–Moyal systematic expansion [11] and arises when one assumes that all the moments of the increments of the stochastic variable of order $\geqslant 3$ are proportional to Δt^r, $r > 1$, where Δt is the time increment. As such, the FPE describes the diffusive motion of Brownian particles under the assumption of *slow* diffusion.

The many-body Fokker–Planck equation in momentum space has been used to describe the dynamics of interacting Brownian particles in the case of superionic conduction [12] and to obtain the conductivity tensor. On a more formal level, it has also been used for the kinetics of a classical gas of particles interacting (in velocity space) through an exclusion principle [13]. The hydrodynamics of interacting Brownian particles has been studied for short-range or screened interactions in [14, 15].

In the present paper, we address the problem of interacting Brownian particles in the viscous limit, when all inertial effects can be neglected due to high friction. Then, starting from the Langevin equation for any one of the N interacting particles—incorporating the force acting on this particle due to all others—one can derive a closed Fokker–Planck equation for the coordinates of all the particles; the former is thus a many-body equation directly written in real space, where the interaction between diffusive particles is clearly displayed in the drift term. Surprisingly enough, we found no previous study using such an approach in the literature.

The FPE is a conservation equation for a probability density P, which can always be written in the form

$$\partial_t P = -\mathrm{div}\, J \tag{1}$$

where J is the probability current. As an example, for a single particle with position $\boldsymbol{x}$ moving in the static external potential $V(\boldsymbol{x})$, the current is the sum of the drift term, $\mu P \partial_{\boldsymbol{x}} V$, and of the diffusion current, $D\partial_{\boldsymbol{x}} P$; in such a case, the equation

$$\partial_t P(\boldsymbol{x}, t) = \partial_{\boldsymbol{x}}[D\partial_{\boldsymbol{x}} P(\boldsymbol{x}, t) + \mu P(\boldsymbol{x}, t)\partial_{\boldsymbol{x}} V(\boldsymbol{x})] \tag{2}$$

where μ is the mobility and D the diffusion constant. Equation (2) gives the probability density for the position of a particle obeying the Langevin equation in its viscous limit, an initial distribution being given.

With several particles, the interesting case occurs when they interact through a given internal force field deriving from a potential V, opening the possibility of competing effects. When V is purely repulsive, no interesting effect is expected: in infinite space, one can guess that the equilibrium state is the uniform one, all probability densities being constant in space. In the opposite case, when the particles attract each other, a competition between diffusion and interaction takes place, which can, at least in principle, produce patterns or structures in space. Obviously enough, the possibility of the latter depends on the features of the interaction potential, namely its strength and its range, and possibly the dimensionality. The competition between drift and diffusion is measured by the ratio D/μ; as a consequence, patterns can be expected at low temperatures, i.e. when the drift term dominates diffusion. If there exists a definite value D_c of D which separates two distinct stationary solutions, the Einstein relation $D/\mu = k_B T$ allows identification of a critical temperature T_c.

The purpose of this paper is to put forward a few results concerning the equilibrium state of FPE for interacting particles, obtained within a mean-field approximation. The paper is

organized as follows. After setting the basic equations relevant to our purpose, we first focus on some potentials allowing an exact treatment of the mean-field equations. In a second step, we discuss the linear stability of the uniform equilibrium state, which is always a solution of the problem. It is seen that instabilities can indeed occur, and the conditions for that are given, yielding the expression of the critical temperature T_c. Eventually, we give the far-from-equilibrium dynamics of the uniform state suddenly cooled below T_c.

For N identical interacting particles, the potential is noted $V(\boldsymbol{x}_1, \boldsymbol{x}_2, \ldots, \boldsymbol{x}_N)$ and the generalization of (2) is written as

$$\partial_t P(\boldsymbol{x}_1, \ldots, \boldsymbol{x}_N, t) = \sum_i \partial_{\boldsymbol{x}_i} [D\partial_{\boldsymbol{x}_i} P(\boldsymbol{x}_1, \ldots, \boldsymbol{x}_N, t) + \mu P(\boldsymbol{x}_1, \ldots, \boldsymbol{x}_N, t)\partial_{\boldsymbol{x}_i} V(\boldsymbol{x}_1, \ldots, \boldsymbol{x}_N)]. \tag{3}$$

In the following the potential is assumed to be the sum of $N(N-1)$ even two-body terms

$$V(\boldsymbol{x}_1, \boldsymbol{x}_2, \ldots, \boldsymbol{x}_N) = \frac{1}{2}\sum_{i\neq j} v(\boldsymbol{x}_i - \boldsymbol{x}_j) \qquad v(\boldsymbol{x}) = v(-\boldsymbol{x}). \tag{4}$$

As anticipated above, (3) is *real-space* FPE, displaying the two-body interaction in the drift term, as contrasted with that used in [12, 13] where the many-body terms involve velocities.

Obviously, the full solution of (3), if known, is of little physical interest, since one is usually interested in the one-particle density $P^{(1)}$ and the pair-density function $P^{(2)}$ (reduced densities of order 1 and 2), defined as

$$\begin{aligned} P^{(1)}(\boldsymbol{x}, t) &= \int \mathrm{d}\boldsymbol{x}_2 \ldots \mathrm{d}\boldsymbol{x}_N P(\boldsymbol{x}, \boldsymbol{x}_2, \ldots, \boldsymbol{x}_N, t) \\ P^{(2)}(\boldsymbol{x}, \boldsymbol{x}', t) &= \int \mathrm{d}\boldsymbol{x}_3 \ldots \mathrm{d}\boldsymbol{x}_N P(\boldsymbol{x}, \boldsymbol{x}', \boldsymbol{x}_3, \ldots, \boldsymbol{x}_N, t). \end{aligned} \tag{5}$$

Due to the many-body interactions, reduced densities obey a hierarchy of the BBGKY type (see e.g. McQuarrie [16]); in the present context, the first equation of this hierarchy is written

$$\partial_t P^{(1)}(\boldsymbol{x}, t) = \partial_{\boldsymbol{x}} \left[D\partial_{\boldsymbol{x}} P^{(1)}(\boldsymbol{x}, t) + (N-1)\mu \int \mathrm{d}\boldsymbol{x}' P^{(2)}(\boldsymbol{x}, \boldsymbol{x}', t)\partial_{\boldsymbol{x}} v(\boldsymbol{x} - \boldsymbol{x}') \right]. \tag{6}$$

Solving this hierarchy is usually impossible; the simplest approximation is of the mean-field type, in which one imposes the form

$$P(\boldsymbol{x}_1, \boldsymbol{x}_2, \ldots, \boldsymbol{x}_N, t) = \prod_{i=1}^{N} p(\boldsymbol{x}_i, t). \tag{7}$$

From (6), the mean-field one-particle probability density p obeys the following equation:

$$\partial_t p(\boldsymbol{x}, t) = \partial_{\boldsymbol{x}} \left[D\partial_{\boldsymbol{x}} p(\boldsymbol{x}, t) + (N-1)\,\mu p(\boldsymbol{x}, t) \int \mathrm{d}\boldsymbol{x}' p(\boldsymbol{x}', t)\partial_{\boldsymbol{x}} v(\boldsymbol{x} - \boldsymbol{x}') \right]. \tag{8}$$

Thus, for $N \gg 1$, the particle density $n(\boldsymbol{x}, t) = Np(\boldsymbol{x}, t)$ is the solution of the integro-differential non-linear equation

$$\partial_t n(\boldsymbol{x}, t) = \partial_{\boldsymbol{x}} \left[D\partial_{\boldsymbol{x}} n(\boldsymbol{x}, t) + \mu n(\boldsymbol{x}, t)\partial_{\boldsymbol{x}} \int \mathrm{d}\boldsymbol{x}' n(\boldsymbol{x}', t) v(\boldsymbol{x} - \boldsymbol{x}') \right]. \tag{9}$$

Clearly, even in this mean-field approximation, finding the solution is not a trivial question.

2. Some exact stationary solutions of the one-dimensional mean-field FPE

In one dimension, all the stationary solutions of (9) give a vanishing current J and are the solutions of

$$D\frac{\mathrm{d}}{\mathrm{d}x}n(x) + \mu n(x)\frac{\mathrm{d}}{\mathrm{d}x}\int_{-\infty}^{+\infty}\mathrm{d}x' n(x')v(x-x') = 0. \tag{10}$$

Because n also appears in the integral, the stationary mean-field solution is not connected in an obvious way to the Boltzmann distribution built with $v(x)$. One could naively believe that, since in the mean-field treatment each particle interacts with $N-1 \simeq N$ other particles through the potential $v(x)$, its equilibrium distribution is $\propto \mathrm{e}^{-N\beta v(x)}$. This turns out to be wrong in general, except for the harmonic potential. Indeed, the one-particle density is obtained by integrating over the coordinates of all the other $N-1$ particles and there is no reason for ensuring that the bare two-body interaction $v(x)$ should spontaneously appear in the Boltzmann way in the one-particle density, even in a mean-field approach. It will be seen that the ordinary Boltzmann factor is recovered only in certain limits (see below). Also note that, since there is no external force field, the equilibrium states—assumed to be independent of the initial condition which naturally implies privileged points—are defined up to an arbitrary translation in space. Otherwise stated, if $n(x)$ is a solution of (10) defined for all x between $\pm\infty$, then $n_{x_0}(x) = n(x-x_0)$, x_0 arbitrary, is also a solution. This degeneracy is discarded by the use of symmetric boundary conditions (see below), or by having in mind that the displayed equilibrium states arise from the initial condition $p(x, t=0) = \delta(x)$.

For some potentials, the solution of equation (10) can be found in closed form. In the following section, we give a few examples and briefly analyse the corresponding solutions.

2.1. The Coulomb potential

We first choose

$$v(x) = v_0\frac{|x|}{\xi} \qquad (v_0 > 0) \tag{11}$$

which, for $d = 1$, mimics the Coulomb potential in the sense that $v(x)$ satisfies the Poisson equation. This is clearly a long-range attractive potential: the force exerted on a given particle is constant in space and is equal to $-(v_0/\xi)\mathrm{sgn}\,x$.

Let us first assume that the particles are confined in the interval $[-L/2, +L/2]$. Introducing the integrated density $q(x)$

$$q(x) = \int_0^x n(x')\,\mathrm{d}x' \tag{12}$$

it is readily seen from (10) and (11) that $q(x)$ obeys the following differential equation ($\beta^{-1} = k_\mathrm{B}T$):

$$q''(x) + \frac{\beta v_0}{\xi}q'(x)[2q(x) - N] = 0. \tag{13}$$

Using the boundary conditions $q(-L/2) = 0$ and $q(+L/2) = N$, a little algebra yields the properly normalized density in the limit $L \to +\infty$

$$n(x) = \frac{N}{2\Delta\cosh^2(x/\Delta)} \qquad \Delta = \frac{2\xi}{N\beta v_0}. \tag{14}$$

This is a peaked distribution, which tends towards $N\delta(x)$ in the limit $N\to +\infty$. Due to the infinite range of the potential, the stationary state is for any D and large N is a cluster of very

small shape as compared to ξ when $\beta v_0 \sim 1$. Note that $p(x)$ is flat at $x = 0$, but decreases approximately like an exponential

$$n(x) \simeq \xi^{-1} N^2 \beta v_0 \mathrm{e}^{-N\beta v_0 |x|/\xi} \equiv \xi^{-1} N^2 \beta v_0 \mathrm{e}^{-N\beta v(x)} \qquad \text{if} \quad x \gg \frac{\xi}{N\beta v_0}. \tag{15}$$

This shows that the Boltzmann behaviour is recovered in the wings of the distribution only.

Note that it is not necessary to introduce a finite interval of length L and subsequently to take the limit $L \to \infty$. Yet, this procedure allows discussion of the invariance by translation mentioned above. Indeed, taking the boundaries at $\pm L/2$ forces the solution $n(x)$ to be even, a symmetry which is conserved when the limit $L \to \infty$ is performed afterwards. On the other hand, by assuming infinite space at the beginning, the calculation yields the same solution (14) as well as all the translated functions $n_{x_0}(x) = n(x - x_0)$ with x_0 being arbitrary. It can be checked that all the functions $n_{x_0}(x)$ indeed satisfy (10).

2.2. The harmonic potential

We now take $v(x) = v_0 x^2/(2\xi^2)$, $v_0 > 0$, another example of long-range attractive potential. In this case, (10) is written as

$$n'(x) + \frac{\beta v_0}{\xi^2} n(x) \int_{-\infty}^{+\infty} (x - x') n(x') \, \mathrm{d}x' = 0. \tag{16}$$

For even $n(x) = n(-x)$, this simplifies to

$$n'(x) + N \frac{\beta v_0}{\xi^2} x n(x) = 0 \tag{17}$$

which gives the solution for the density

$$n(x) = \frac{N}{\sqrt{2\pi}\Delta} \mathrm{e}^{-x^2/(2\Delta^2)} \qquad \Delta = \frac{\xi}{\sqrt{N\beta v_0}}. \tag{18}$$

Note that the expression (18) is simply of the form $\propto \mathrm{e}^{-N\beta v(x)}$, which is the Boltzmann distribution for a single particle elastically bound with N others. The fact that this is true for all N and x is clearly characteristic of the harmonic potential. Again, it is readily verified that all the functions $n(x - x_0)$ satisfy (16) with x_0 arbitrary.

2.3. Polynomial potentials

The harmonic potential treated above immediately gives the clue for solving the same problem with any potential of the polynomial type

$$v(x) = \sum_{r \geqslant 1} c_r x^r. \tag{19}$$

With this kind of potential, (10) assumes the form

$$n'(x) + \beta n(x) \sum_{r \geqslant 1} r c_r \int_{-\infty}^{+\infty} (x - x')^{r-1} n(x') \, \mathrm{d}x' = 0. \tag{20}$$

By rearranging the terms in the integral, this can be rewritten as

$$n'(x) + \beta n(x) \sum_{r \geqslant 1} \gamma_r(x) f_r = 0 \tag{21}$$

where the $\gamma_r(x)$ are definite polynomials and where the quantities f_r are the moments of $n(x)$

$$f_r = \int_{-\infty}^{+\infty} x^r n(x) \, \mathrm{d}x. \tag{22}$$

Now, (21) can be formally integrated to give a function $p(x)$ containing the parameters f_r

$$n(x) = \mathrm{e}^{-\beta \sum_{r\geqslant 0} \Gamma_r(x) f_r} \tag{23}$$

Γ_r being definite functions depending on $v(x)$. By reporting this expression in (22), one can write as many equations as necessary to find f_r and eventually obtain the explicit expression of $n(x)$. Clearly, the latter is not *a priori* of the form $\propto \mathrm{e}^{-N\beta v(x)}$.

As an example, let us consider the quartic potential

$$v(x) = v_0 \left[g \left(\frac{x}{\xi} \right)^2 + \left(\frac{x}{\xi} \right)^4 \right]. \tag{24}$$

This potential is purely attractive if $g > 0$; otherwise, it is repulsive for x between $\pm\sqrt{[-g/2]}$ and attractive elsewhere. Inserting this potential in (20) and integrating, one finds

$$n(x) = C\mathrm{e}^{-\beta v_0 [(g\xi^2 f_0 + 6 f_2)\, x^2/\xi^4 + f_0 x^4/\xi^4]}. \tag{25}$$

f_0 is equal to N, whereas the unknown quantities C and f_2 can be derived from the two equations

$$2C \int_0^{+\infty} \mathrm{e}^{-\beta v_0 [(gN + f_2/\xi^2) X^2 + N X^4]}\, \mathrm{d}X = N \qquad 2C\xi^2 \int_0^{+\infty} X^2 \mathrm{e}^{-\beta v_0 [(gN + f_2/\xi^2) X^2 + N X^4]}\, \mathrm{d}X = f_2. \tag{26}$$

Note that the expression (25) is not $\propto \mathrm{e}^{-N\beta v(x)}$, except if f_2 is negligible compared with $N\xi^2$ (see below). The above integrals can be expressed [17] with the Weber functions $\mathcal{D}_\nu$

$$\sqrt{\pi} C (2N\beta v_0)^{-1/4} \mathrm{e}^{A^2/4} \mathcal{D}_{-1/2}(A) = N \qquad \frac{\sqrt{\pi}}{2} C\xi^2 (2N\beta v_0)^{-3/4} \mathrm{e}^{A^2/4} \mathcal{D}_{-3/2}(A) = f_2. \tag{27}$$

where the constant A is

$$A = \frac{\beta v_0}{2N} (gN + f_2/\xi^2)^2. \tag{28}$$

For arbitrary N, these equations can be numerically solved to provide the two parameters C and f_2. On the other hand, when N is very large, one can find directly asymptotic expressions of the integrals appearing in (26). By doing so and coming back to the mean-field density $n(x)$, one gets according to the sign of g

$$n(x) \simeq N\xi^{-1} \left(\frac{2g\beta v_0 N}{\sqrt{\pi}} \right)^{1/2} \mathrm{e}^{-N\beta v(x)} \qquad (g > 0) \tag{29}$$

$$n(x) \simeq N\xi^{-1} \left(\frac{|g|\beta v_0 N}{\sqrt{2\pi}} \right)^{1/2} \mathrm{e}^{-N\beta v_0 g^2/4} \mathrm{e}^{-N\beta v(x)} \qquad (g < 0). \tag{30}$$

This shows that the Boltzmann distribution is recovered only in the limit $N \gg 1$. For positive g, one has a single cluster with a width $\sim (N\beta v_0)^{-1/2}\xi$. For negative g, two peaks arise, both having the latter width and separated by $\sqrt{-2g}\xi$.

Note that, in any case with $\beta v_0 \sim 1$, the mean-field stationary state for large N is a compact cluster with a very small size compared with the characteristic length ξ of the potential.

3. Linear stability analysis of the uniform state

In the previous section, we displayed several potentials allowing an exact explicit expression for the non-uniform equilibrium state with a vanishing current. On the other hand, (10) always trivially has the uniform state as a solution. All this means that several solutions can exist and the question arises to settle which of them can indeed be realized for a given ratio D/μ. As shown by numerical studies [1, 2], various structural phase transitions can arise in the lattice version of this problem. The aim of this section is to analyse the linear stability of the uniform solution n_0 of the mean-field equation (10) in any dimension. Setting $n(\boldsymbol{x}, t) = n_0 + \delta n(\boldsymbol{x}, t)$ and discarding all terms of order greater than one, one obtains

$$\partial_t \delta n(\boldsymbol{x}, t) = D\partial_{\boldsymbol{x}}^2 \delta n(\boldsymbol{x}, t) + \mu n_0 \partial_{\boldsymbol{x}} \int \mathrm{d}\boldsymbol{x}' \delta n(\boldsymbol{x}', t) \partial_{\boldsymbol{x}} v(\boldsymbol{x} - \boldsymbol{x}'). \tag{31}$$

This linear equation can now be analysed by introducing the Fourier transforms

$$\rho(\boldsymbol{q}, t) = \int \mathrm{d}\boldsymbol{x}\, \mathrm{e}^{-\mathrm{i}\boldsymbol{q}\boldsymbol{x}} \delta n(\boldsymbol{x}, t) \qquad \tilde{v}(\boldsymbol{q}) = \int \mathrm{d}\boldsymbol{x}\, \mathrm{e}^{-\mathrm{i}\boldsymbol{q}\boldsymbol{x}} v(\boldsymbol{x}). \tag{32}$$

and it is readily seen that all the eigenmodes of (31) are of the form $\mathrm{e}^{-\omega(q)t}$, with $\omega(\boldsymbol{q})$ given by the dispersion relation

$$\omega(\boldsymbol{q}) = [D + \mu n_0 \tilde{v}(\boldsymbol{q})]\, \boldsymbol{q}^2 \equiv D_{\mathrm{eff}}(\boldsymbol{q}) \boldsymbol{q}^2. \tag{33}$$

D_{eff} plays the role of an effective $\boldsymbol{q}$-dependent diffusion constant; it can be said that, due to the interactions, Fick's law is no longer a local law. Setting

$$v(x) = v_0 \phi(x/\xi) \qquad \phi(0) > 0 \quad x = |\boldsymbol{x}| \quad q = |\boldsymbol{q}| \tag{34}$$

the dispersion law (33) in d dimensions can be rewritten as

$$\omega(q) = D\left[1 + \beta v_0 n_0 \xi^d U_d(q\xi)\right] q^2 \tag{35}$$

where U_d is a dimensionless function. More precisely, one has (J_0 is the ordinary Bessel function)

$$U_1(\kappa) = 2\int_0^{+\infty} \phi(X) \cos(\kappa X)\, \mathrm{d}X \qquad U_2(\kappa) = 2\pi \int_0^{+\infty} X\phi(X) J_0(\kappa X)\, \mathrm{d}X \tag{36}$$

$$U_3(\kappa) = \frac{4\pi}{\kappa} \int_0^{+\infty} X\phi(X) \sin(\kappa X)\, \mathrm{d}X. \tag{37}$$

Equation (35) shows that the uniform solution is unstable against a deformation with a wavevector $\boldsymbol{q}$ satisfying

$$k_{\mathrm{B}}T + n_0 \xi^d v_0 U_d(q\xi) < 0. \tag{38}$$

Clearly, such a condition cannot be satisfied for a purely repulsive potential, since both v_0 and U_d are positive quantities[1]: for repulsive forces, the uniform state is always stable, as anticipated on physical grounds in section 1.

When v is attractive at short distances, v_0 is negative. The possibility of instability then depends only on the precise behaviour of the dimensionless Fourier transform U_d. For very short-range potentials, $U_d(\kappa)$ is expected to be positive for all κ. The instability condition can then be rewritten in a more transparent form

$$k_{\mathrm{B}}T < n_0 \xi^d |v_0| U_d(q\xi) \qquad v_0 < 0. \tag{39}$$

[1] When $\phi(X)$ is a positive function, U_d is bounded below by a positive (possibly diverging) integral.

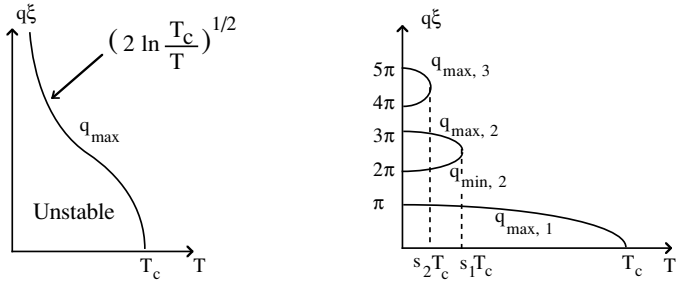

Figure 1. Schematic representation of the instability domains for the Gaussian potential (41) (left, below $q_{\max}$) and for the square potential (45) (right, pockets).

If, in addition, U_d is a monotonic decreasing function, instability occurs at large wavelengths provided that the temperature is low enough. More precisely, provided that $U_d(0)$ is finite (short-range potential), one can define a critical temperature T_c

$$k_B T_c = n_0 \xi^d |v_0| U_d(0). \tag{40}$$

For $T < T_c$, there exists a finite interval $[0, q_{\max}]$ in which the uniform state is unstable. $q_{\max}$ is a function of the density n_0 and the temperature. Assuming that U_d (0) is of order unity, (40) means that the critical temperature is such that the thermal energy is of the order of the effective interaction energy.

The existence of an upper $q_{\max}$, below which the uniform solution is unstable, is easily understood on physical grounds. For a small disturbance having a large wavelength compared to the range of the potential, particles in excess tend to attract each other more firmly, increasing holes in the density. On the other hand, when the wavelength is quite small, the inhomogeneities are easily washed out since holes and particles all interact.

As an example, let us consider the d-dimensional Gaussian attractive potential

$$v(x) = v_0 \, \mathrm{e}^{-x^2/(2\xi^2)} \qquad v_0 < 0. \tag{41}$$

In this case, one has

$$k_B T_c = (2\pi)^{d/2} n_0 \xi^d |v_0| \tag{42}$$

and $q_{\max}$ is given by

$$q_{\max} = \xi^{-1} \left(2 \ln \frac{T_c}{T} \right)^{1/2} \qquad T \leqslant T_c \tag{43}$$

which entails that

$$q_{\max} \sim (T_c - T)^{1/2} \qquad T \lesssim T_c. \tag{44}$$

These last results are depicted in the left-hand side of figure 1. The same conclusions still qualitatively hold if a repulsive core is added (e.g. 6–12 Lennard-Jones or Morse potential). This only affects the large-q behaviour of $\tilde{v}$ and does not change the results.

When the potential has a sharp cut-off, its Fourier transform has an oscillatory behaviour at relatively small wave numbers and an interesting phenomenon occurs. To be specific, let us take the following square potential

$$v(x) = \begin{cases} v_0 & \text{if } |x| < \xi/2 \\ 0 & \text{otherwise} \end{cases} \qquad v_0 < 0. \tag{45}$$

Here we find $k_B T_c = n_0 \xi |v_0|$. Now, let us note X_k are the *abscissae* of the maxima of $(\sin X)/X$ and $s_k \equiv (\sin X_k)/X_k$ ($X_0 = 0, s_0 = 1$). Then, for $s_1 T_c < T < T_c$, a single instability interval

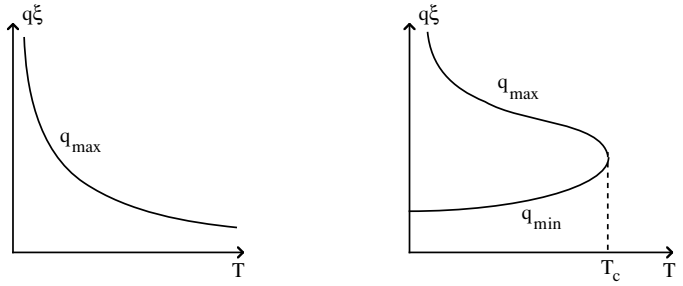

Figure 2. Schematic representation of the instability domain for the Coulomb potential (11) (left, below $q_{\max}$) and the inverted Morse potential (47) (right, between $q_{\min}$ and $q_{\max}$).

arises, $[q_{\min,1} = 0, q_{\max,1}]$. When T decreases, another interval $[q_{\min,2}, q_{\max,2}]$ is found when $s_2 T_c < T < s_1 T_c$, and so on. The situation is depicted in figure 1. Thus, for a short-range potential with a sharp cut-off, several disjoint instability intervals are successively obtained when the temperature decreases.

If $U_d(0)$ is infinite, T_c is also formally infinite; this means that the uniform solution is unstable at small q for *any* temperature (see figure 2, left). For instance, for the one-dimensional Coulomb potential (11), one has (after regularization) $U_1(\kappa) = 2/\kappa^2$, so that

$$q_{\max} = \xi^{-1}\sqrt{\frac{2n_0\xi v_0}{k_B T}} \qquad \forall T. \tag{46}$$

The same holds true for higher dimensions, since $U_d(\kappa)$ is for any d proportional to κ^{-2}.

In the preceding examples, the first instability interval, when it exists, arises around $q = 0$. This is, as explained above, a physical consequence of the fact that the potential is purely attractive (the fact that T_c is finite or not is a consequence of range only). Another interesting situation is when competing effects are present, i.e. when v is attractive at a short distance and repulsive at long distance; this means that two particles are bound by a potential barrier, but can dissociate when one of them is given enough energy. As an example, let us consider the *inverted* $3d$ Morse potential

$$v(x) = v_0\left[e^{-2(r-r_0)/\xi} - 2e^{-(r-r_0)/\xi}\right] \qquad v_0 < 0\ . \tag{47}$$

In such a case, T_c is again finite and the instability interval for q is of the form $[q_{\min}, q_{\max}]$; it grows around a *finite* value (which gives $U_3(q\xi)$ its secondary minimum) and is a consequence, at intermediate wavelengths, of the interplay between attraction at short distances and repulsion at large distances. This instability domain is schematized in figure 2 (right). Quite naturally, stability of the uniform state against long wavelength deformations is recovered, due to the long distance repulsive behaviour of the potential.

4. Numerical study of the Gaussian attractive case

From the arguments and results given in the two previous sections, we expect that for a Gaussian attractive case (an example of short-range potential), two equilibrium solutions exist; the uniform one, which is unstable against long wavelength deformations when $T < T_c$, where T_c is given by (42), and a non-uniform distribution, which we were unable to find analytically in a closed form. The aim of this section is to give numerical results for the one-dimensional Gaussian potential. It is shown below that the predicted transition between

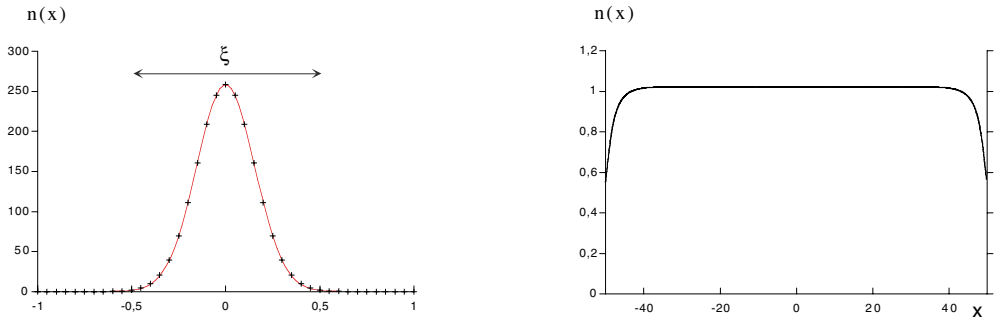

Figure 3. Equilibrium states for the Gaussian potential (left: $T/T_c = 0.9$, right: $T/T_c = 1.1$); the length of the box is $L = 100\,\xi$ and $N = 100$ ($n_0 = 1$). On the left curve, the crosses are the results from the static algorithm whereas the solid line is the Gaussian approximation defined in the text. ξ is the unit length; note the different horizontal and vertical scales.

these two states is indeed quite sharp when T crosses T_c and that, in addition, a hysteretic behaviour occurs.

We choose $v(x) = v_0 e^{-x^2/(2\xi^2)}$ ($v_0 < 0$), which yields $\tilde{v}(q) = \sqrt{2\pi}\xi v_0 e^{-\xi^2 q^2/2}$. The instability condition (38) gives the critical temperature (see (40))

$$T_c = \sqrt{2\pi} n_0 \xi |v_0| / k_B. \tag{48}$$

In order to analyse the equilibrium state(s) $n(x)$ arising in the mean-field treatment with the Gaussian potential, we used two numerical procedures. The first is a self-consistent iterative procedure for the equilibrium equation (10), hereafter called the static algorithm. The second (called the dynamical algorithm) numerically solves the one-dimensional version of the full equation (9), starting from a given initial condition $n(x, t = 0)$, and gives the non-equilibrium evolution of the system.

With the static algorithm, we start from a trial density function $n^{(0)}$ and then iterate according to

$$n^{(k+1)}(x) = Z^{-1} e^{-\beta \int_L dy\, n^{(k)}(x) v(y-x)} \tag{49}$$

where Z is the normalization constant. Convergence is reached when the following quantity

$$\int_L dx \left(\frac{n^{(k+1)}(x) - n^{(k)}(x)}{n^{(k+1)}(x)} \right)^2 \tag{50}$$

becomes much less than unity. Strict boundary conditions have been used, namely $j(0, t) = j(l, t) = 0$.

These calculations first allow checking for the existence of the sharp transition occurring at T_c when the temperature decreases, starting with the uniform state; second, they reveal a hysteretic behaviour, i.e. when the temperature *increases*, starting from the localized state (one cluster), the transition from the localized state to the uniform one occurs at another temperature $T_c^* > T_c$.

Figure 3 displays two typical density profiles (uniform versus localized cluster), just above and below T_c obtained from this static algorithm. Since the width of the localized state turns out to be a little bit smaller than the range ξ of the potential, the central part of the cluster can be safely approximated by a Gaussian; indeed, when one expands the potential near $x/\xi \sim 0$, the harmonic potential is recovered (if instead of a Gaussian potential, one chooses $v(x) = v_0 e^{-|x|/\xi}$, the central shape of the localized cluster is $1/\cosh^2 x$, as it must be (see (14)) since near the centre this potential is essentially the Coulomb potential). Obviously, such an approximation cannot properly represent the tails of the equilibrium density.

In order to characterize the transition, we introduce two quantities, ε and λ defined as

$$\varepsilon(T/T_c) = \frac{1}{N}\int_L \mathrm{d}x\,\mathrm{d}x' n(x)n(x')v(x-x') \tag{51}$$

and

$$\Delta^2(T/T_c) = \frac{1}{N}\int_L \mathrm{d}x\, x^2 n(x) - \left[\frac{1}{N}\int_L \mathrm{d}x\, x n(x)\right]^2. \tag{52}$$

ε represents the mean-field interaction energy per particle; Δ measures the spatial width of the cluster. For the uniform state one has $\varepsilon_{\mathrm{unif}} = (N/L)\int_L \mathrm{d}x\, v(x) \sim N(\xi/L)v_0$ and $\Delta_{\mathrm{unif}} \sim L \gg \xi$; in contrast, for the localized state, $\varepsilon_{\mathrm{loc}} \sim N v_0$ and $\Delta_{\mathrm{loc}} \lesssim \xi$. For an infinite system, the ratio $\varepsilon_{\mathrm{loc}}/\varepsilon_{\mathrm{uniform}}$ vanishes, so that ε can play the role of an order parameter.

The hysteresis is obtained as follows. For each given temperature, the starting point is the solution found in the previous run at a slightly different temperature. After a first sequence where T/T_c decreases step by step down to 0.2, the procedure is reversed, in that T/T_c increases, and the iterative procedure starts again from the localized solution obtained for the previous value of T/T_c. It is found that the inverse transition does not occur at $T/T_c = 1$, but at a *higher* temperature T_c^*.

Clearly, for $T < T_c$, several solutions can exist. Since the width of the single peak solution is a bit smaller than the range ξ of the potential, one can guess that there also exists a solution with two peaks separated by a distance much larger than ξ. This is confirmed by the numerical calculations: starting with a trial function having two separate peaks, the calculation converges towards a stable solution having the same features. One can thus claim that, on the low-temperature side, localized solutions exist displaying $j = 1, 2, 3, \ldots$, peaks. Each of these solutions has its own temperature $T_{c,j}^*$. The corresponding typical hysteretic cycles are shown in figure 4 for the 'order parameter' ε for the one-, two- and three-peak solutions.

The possibility of n-peak solutions is confirmed by the dynamic algorithm (it was checked that the latter eventually yields the same equilibrium solutions as the static equilibrium). This allows the conclusion that a given j-peak solution is linearly stable for $T_c < T < T_{c,j}^*$. Note that the linear stability of the n-peak solutions above T_c is not contrary to the results obtained in section 3; all this simply means that, in the region $T_c < T < T_{c,j}^*$, both the uniform state and the localized state(s) are stable against *small* perturbations.

Defining the entropy as $S = -\int_L \mathrm{d}x\, n(x)\ln[n(x)/n_0]$, it is seen that the one-peak solution is the one having the lowest free energy $F = \varepsilon - TS$. It must be noted that each kind of state has its own relevant physical parameters. For the uniform state, the relevant parameters are $v_0, \xi, n_0 = N/L$ and the critical temperature found by the linear stability analysis is a function of these parameters. For the localized state, the relevant parameters are v_0, ξ and N, the number of particles. Indeed, for this state, edge-effects become irrelevant when $\xi \ll L$: in this sense L becomes arbitrary so that n_0 and N are in fact independent variables.

The physical reason for the hysteresis can be understood as follows. In the uniform state, a given particle interacts with a small (microscopic) number of particles ($\sim n_0\xi$); in contrast, in the localized state, a single particle interacts with a large number ($\sim N$), macroscopic in the sense that all the particles effectively interact with any one of them (note that this also originates from the fact that the particles are of zero radius). The condition for the uniform-to-localized transition is expressed by $k_B T_c \sim n_0\xi|v_0|$ (see (40)). For the inverse transition, one can expect that a somewhat similar condition also holds true, so that T_c^* is an increasing function of N (and is independent of n_0). It is likely that with pointlike particles T_c^* goes to infinity with N; in contrast, with finite-size particles, one can figure out that T_c^* saturates at very large N. As a whole, the hysteretic behaviour is a consequence of this parameter cross-over between the two kinds of steady states.

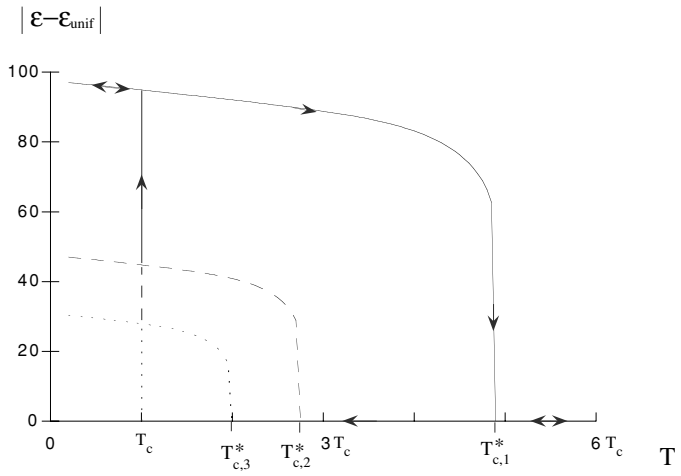

Figure 4. $|\varepsilon - \varepsilon_{\mathrm{unif}}|$ versus T: hysteresis cycle for the uniform–localized transition. Solid line: one-peak branch, dashed line: two-peak branch, dotted line: three-peak branch.

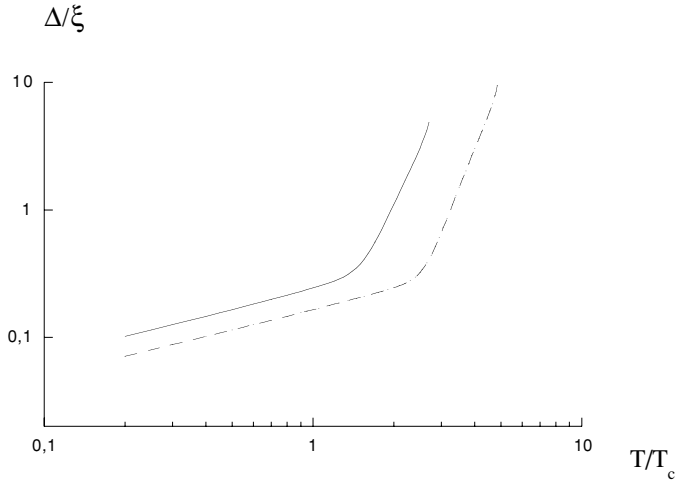

Figure 5. Δ versus T/T_{c}, for $N = 50$ (solid line) and $N = 100$ (dashed line). The two curves display two well-separated regimes; at low temperature, $\Delta \propto T^{1/2}$, whereas at high temperature, Δ still follows a power law, but with an exponent $\simeq$5.4. Both curves end at their own localized–uniform transition temperature.

These facts are illustrated by looking at the width Δ of the cluster in the localized state, displayed in figure 5 where Δ is plotted as a function of the relevant variables for the uniform state (as they naturally arise in the linear stability analysis in section 3). Indeed, choosing $N = 50$ or 100 with fixed n_0 gives two different curves.

In the localized state, the width Δ of the cluster displays a cross-over between the two regimes. On the low-T side, one finds approximately $\Delta \propto T^{1/2}$. This behaviour is the same as for the harmonic case (see section 2.2), which suggests that a Gaussian approximation is valid in the low-T region. Indeed, one can compare Δ with the analytic expression (18) obtained for the harmonic case (see figure 6). The agreement turns out to be quite good and this allows claiming that a Gaussian approximation provides a very accurate description of the localized

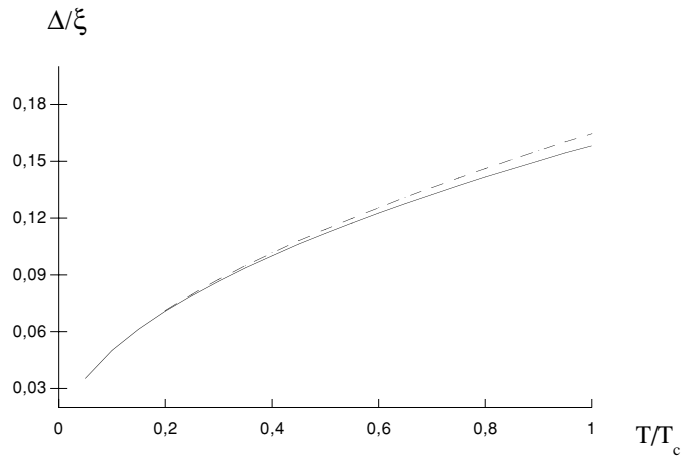

Figure 6. Comparison between the Gaussian approximation (dashed line) and the numerical results (solid line) for the dependence of the width versus the temperature, in the low-T region ($N = 100$).

state arising in the low-T region. For the second regime ($T_c < T < T_c^*$), the width of the cluster becomes of the same order or even greater than the potential range, so that the effective potential cannot be well represented by a harmonic approximation. Indeed, the increase in the cluster width with T no longer displays a Gaussian behaviour, but still follows a power law.

5. Dynamics of a system of particles interacting through the Gaussian potential

In the previous mean-field analysis, it was shown that Brownian particles interacting through a Gaussian potential can have several steady states when $T_c < T < T_c^*$. The system will converge towards one of those states, depending on the initial condition. It can be expected that, under a strong perturbation, the former is able to shift from one steady state to another, without changing the two-phase space parameters (T/T_c and N).

Here we give a few results obtained from the dynamical algorithm for a set of $N = 100$ particles starting in the uniform state at $T/T_c = 0.5$. The length of the box is $L = 100\,\xi$. This represents a case where the system, being in its stable uniform state at a given $T > T_c$, is cooled infinitely quickly below its critical temperature.

We find that the dynamics is a succession of steps, each of them being a metastable state. Each *plateau* has a free energy lower than that of the preceding step. The mean energy per particle is plotted in figure 7 as a function of time. In order to be complete, some corresponding density profiles at different times are shown in figure 8.

These plots show that the dynamics is a succession of metastable states with a given number of peaks of high density (13-peak state, seven-peak state, five-peak state, three-peak state). The lifetimes of these states rapidly increase when the number of peaks gets lower (note the horizontal logarithmic scale in figure (7).

Because of the computational time, we were unable to obtain the one-peak state. From static computations, it is believed that this state is expected to be the final one, although there is no evidence that the two algorithms have the same attraction basins. Moreover, the one-peak state is not the only stable state: we have checked that there also exist stationary two-peak and three-peak states, a fact which seems nearly obvious on physical grounds since the distance between two neighbouring peaks is much larger than the range ξ when no dynamics can occur.

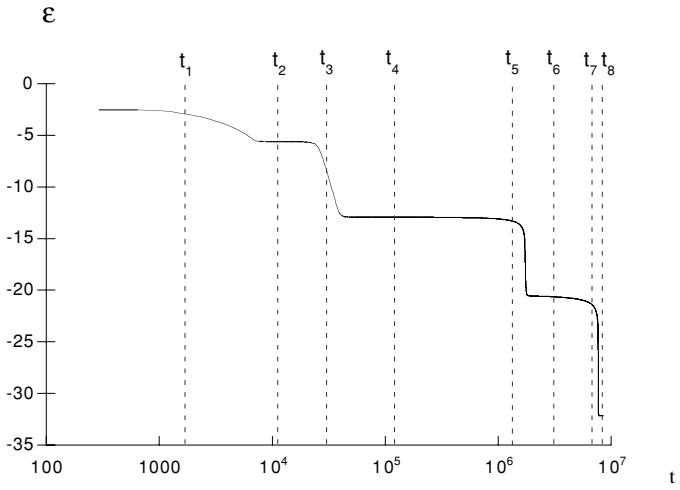

Figure 7. Time evolution of the mean energy per particle ε, starting with the uniform state suddenly cooled below the critical temperature ($T/T_c = 0.5$ and $N = 100$). Note the horizontal logarithmic scale; the time unit is $\xi/(\mu n_0|v_0|)$.

From the time-dependent density profiles (figure 8), we see that 'nucleation' always occurs at the boundaries of the box. This is easily understood, since a particle near this boundary is pulled from one side only, as opposed to a particle located in the bulk. This effect would disappear with periodic boundary conditions, indicating that the nucleation can only occur around an inhomogeneity.

It is also interesting to follow the annihilation of the peaks. As an example, one goes from 13 to 7 peaks via the diffusion of the even peaks into the odd peaks. Generally speaking, it turns out that the transition towards a state having fewer peaks proceeds through the absorption of 'weak' peaks into strong peaks. The actual value of the density between the peaks, even when it is extremely small, turns out to be of first importance in this mechanism of coalescence.

6. Conclusion

In this paper, we have studied properties of the N-body Fokker–Planck equation within a mean-field approximation. Our aim was to analyse the properties of the steady state—which is a uniform density gas when interactions are set to zero—as a function of the features of the interaction potential. The linear stability analysis of the uniform state allowed a statement of the condition for a phase transition as a result of the competing effects due to attractive interaction and diffusive spreading. In particular, it was shown that the uniform phase is always unstable for non-summable attractive potentials, the critical temperature being infinite. In this latter case, analytical results have been given for specific potentials (1D-Coulombian, harmonic, polynomials etc.), all yielding an aggregated steady state. Previous studies with a lattice framework revealed the possibility of phase transition, a phenomenon which also arises in the continuous version of the problem.

For an attractive short-range interaction, the above stability condition was interpreted as phase transition occurring at a finite T_c. This transition was more thoroughly studied by numerical computations in a definite case (Gaussian potential) and turns out to be of the first

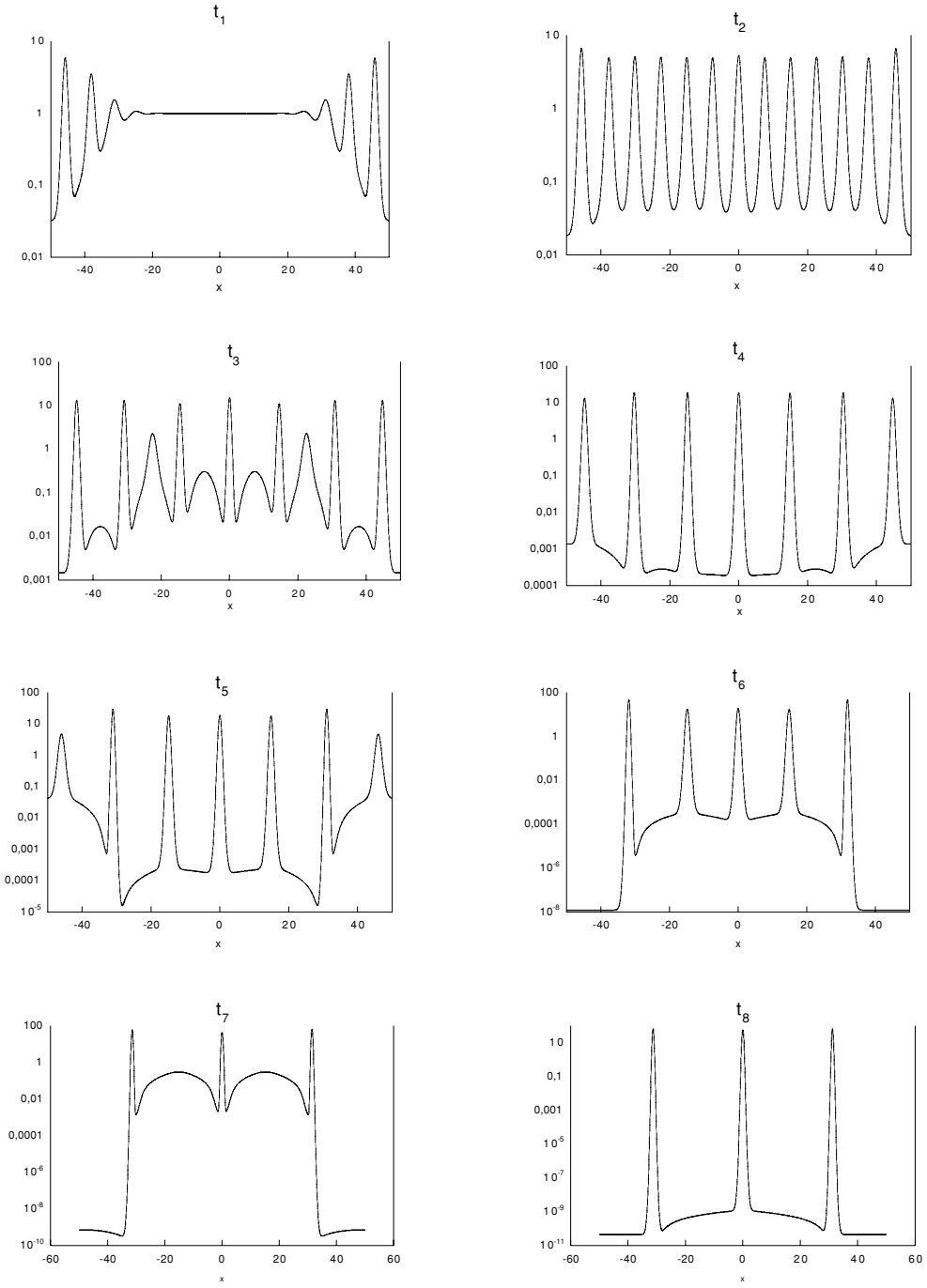

Figure 8. Sequence of the density profile at different times, starting from the uniform state cooled below T_c.

order and hysteretic, the low temperature state being an inhomogeneous state having one or several peaks of high density.

The far-from-equilibrium dynamics was numerically computed for the Gaussian potential, starting from the uniform state suddenly cooled below T_c. The relaxation proceeds through a sequence of *plateaux* displaying a given decreasing number of peaks, each of the former having a longer and longer lifetime as time goes on. Each of these steps can be viewed as a metastable state.

Obviously enough, the considered problem requires further investigations. The most obvious one is further analysis of the relevance of the mean-field approach. If one expects that the mean-field results should be basically valid for long-range potentials and high-space dimensionality, their correctness for short-range potentials has to be checked by using more refined approximations from N-body general methods.

Acknowledgment

We are indebted to Julien Vidal for a careful reading of the manuscript and for his most valuable remarks.

References

[1] Williams E D, Cunningham S L and Weinberg W H 1978 A determination of adatom–adatom interaction energies: application to oxygen chemisorbed on the tungsten (110) surface *J. Chem. Phys.* **68** 4688
[2] Ching W Y, Huber D L, Fishkis M and Lagally M G 1978 Monte Carlo modeling of phase changes in the chemisorption system O/W (110) *J. Vac. Sci.* **15** 653
[3] Tringides M C and Gomer R 1984 A Monte Carlo study of oxygen diffusion on the (110) plane of tungsten *Surf. Sci.* **145** 121
[4] Gomer R 1990 Diffusion of adsorbates on metal surfaces *Rep. Prog. Phys.* **53** 917
[5] Tringides M C and Gomer R 1992 Adsorbate–adsorbate interaction effects in surface diffusion *Surf. Sci.* **265** 283
[6] Zaluska-Kotur M A and Turski L A 1994 Diffusion coefficient for interacting lattice gases *Phys. Rev.* B **50** 16102
[7] Gortel Z W, Zaluska-Kotur M A and Turski L A 1995 Diffusion coefficient for interacting lattice gases: Repulsive interactions *Phys. Rev.* B **52** 16920
[8] Aslangul Cl 1996 Analytical study of an asymmetric 1D statistical model for chemical reactions *Physica* A **231** 687
[9] Zhdano V P and Kasemo B 1994 Kinetic phase transitions in simple reactions on solid surfaces *Surf. Sci. Rep.* **20** 111
[10] Kehr K W and Binder K 1984 Simulation of diffusion in lattices gases and related kinetic phenomena *Applications of Monte Carlo Methods in Statistical Physics* (*Topics in Current Physics* vol 36) ed K Binder (Berlin: Springer) p 181
[11] Gardiner C W 1990 *Handbook of Stochastic Methods* (Berlin: Springer)
[12] Boughaleb Y 1988 Relation entre les proprietes dynamiques et structurales des conducteurs superioniques *J. Phys. France* **49** 2077
[13] Kaniadakis G and Quarati P 1993 Kinetic equation for classical particles obeying an exclusion principle *Phys. Rev.* E **48** 4263
[14] Hess W and Klein R 1983 Generalized hydrodynamics of systems of Brownian particles *Adv. Phys.* **32** 173
[15] Nagele G, Medina-Noyola M and Klein R 1988 Time-dependent self diffusion in model suspensions of highly charged Brownian particles *Physica* A **149** 123
[16] McQuarrie D A 1973 *Statistical Mechanics* (New York: Harper and Row)
[17] Erdelyi A, Magnus W, Oberhettinger F and Tricomi F G 1954 *Tables of Integral Transforms* vol 1 (New York: McGraw-Hill)